Time-Domain Envelope Measurement Technique with Application to Wideband Power Amplifier Modeling

Christopher J. Clark, George Chrisikos, *Member, IEEE,* Michael S. Muha, Andrew A. Moulthrop, and Christopher P. Silva, *Senior Member, IEEE*

***Abstract*— This paper presents a new time-domain measurement technique for repetitive microwave signals that is applied to modeling wideband power amplifiers. The measurement technique concept consists of recording the microwave signal after conversion to baseband using a calibrated downconverter, which improves measurement accuracy compared to measurements at the carrier frequency. The modeling section describes how such time-domain measurements can be used to model wideband signal effects in nonlinear power amplifiers. The commonly used memoryless envelope model is limited to use on narrowband signals. A new model is developed which includes a filter before the memoryless nonlinearity to capture the memory effects associated with wideband signals. It is demonstrated that the accuracy of wideband signal simulations can be improved by optimizing the model parameters based on time-domain measurements of wideband signals.**

***Index Terms*—ARMA models, low-pass equivalent signals, microwave time-domain measurements, nonlinear amplifier modeling.**

I. Introduction

COMMUNICATIONS system simulations often employ block models to predict distortion created by their nonlinear components. In these models, the nonlinear components are characterized in terms of input and output complex envelopes. A low-pass equivalent (LPE) representation of signals is used to avoid the high sampling rate required at the carrier frequency. This powerful method is capable of analyzing systems driven by signals ranging from single-tone sinusoids to complex digitally modulated carriers. The memoryless envelope transfer model has been commonly used to represent nonlinear power amplifiers and is implemented in commercial CAD programs.[1,2] The power amplifier is often represented by nonlinear amplitude (AM/AM) and phase (AM/PM) functions in either polar or quadrature form.

Assumptions in the mathematical formulation of the memoryless envelope transfer model limit it to narrowband applications. The AM/AM and AM/PM are measured in the center of the band and assumed to be constant (memoryless) over the bandwidth of the simulated signal. Other models have been proposed for simulation of wideband signals [1], but none of them seems to provide an efficient implementation with easily measured parameters. As a consequence, the ability to make wideband, accurate measurements of the complex envelope is essential for the full understanding of nonlinear device operation.

A new method is presented here to measure directly and accurately the time-domain complex envelope of wideband signals. In this method, the microwave signal is mixed down to baseband, where it is an LPE waveform [2], having both in-phase and quadrature components, which are recorded by means of a Hewlett-Packard microwave transition analyzer (MTA). The downconverting receiver frequency response is then removed from the recorded waveforms by application of the baseband double-sideband mixer characterization method [3], providing an accurate LPE representation of the original microwave signal.

In this paper, a new model of a 20-GHz traveling-wave tube amplifier (TWTA) is presented that has been optimized using time-domain LPE waveforms. A variety of wideband waveforms are used to demonstrate the capability of this model and compare it to more traditional models.

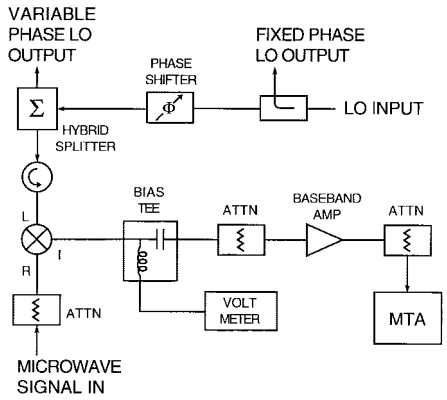

Fig. 1. Simplified receiver block diagram.

II. Test System Configuration

The basic measurement system consists of a downconverting receiver followed by an MTA as shown in Fig. 1. The

Manuscript received March 27, 1998; revised September 3, 1998.

The authors are with The Aerospace Corporation, Los Angeles, CA 90009-2957 USA (e-mail: chris.j.clark@aero.org).

Publisher Item Identifier S 0018-9480(98)09233-3.

[1] *OMNISYS*™, *Series IV Design Suite*, Hewlett-Packard, HP EESof Division, 5601 Lindero Canyon Road, Westlake Village, CA 91362.

[2] *SPW*™, *Signal Processing Worksystem*, Comdisco Systems, Inc., 919 Hillsdale Blvd., Foster City, CA 94404.

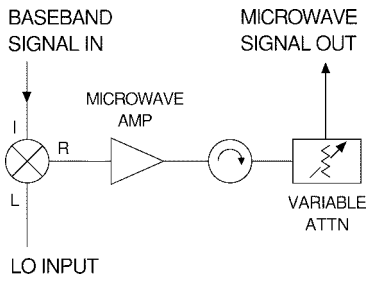

Fig. 2. Simplified transmitter block diagram.

dc level, which corresponds to the Fourier component at the carrier frequency, is measured separately by means of a bias tee and a voltmeter at the output of the downconverting mixer. This is required since the baseband amplifier blocks the dc component. Note that a digital storage oscilloscope could be used in place of the MTA, but the MTA has advantages such as an extensive internal calibration routine and the capability of locking to an external 10-MHz reference.

The microwave signal to be measured can have any arbitrary repetitive phase or amplitude modulation imposed upon it, but it must be accompanied by an unmodulated carrier to feed the receiver's local oscillator (LO) input. The receiver has two coherent LO outputs, a fixed phase and a variable phase LO. These outputs can be used with a transmitter (see Fig. 2), and are required for the calibration procedure outlined below that uses both the transmitter and a test mixer. The stability requirements on the carrier need not be high because its phase noise is canceled by the coherent downconversion. The baseband modulation signal, however, must be stable, preferably with a 10-MHz reference output to be used by the MTA as an external reference. The modulating source can be used to trigger the MTA if a separate trigger output is not available.

When the equipment is configured as shown in Fig. 1, the downconverted signal is recorded at an arbitrary relative carrier phase between the microwave signal source and the receiver, constituting the uncorrected in-phase component of the LPE signal. The phase shifter is then adjusted by 90° and the downconverted signal is again recorded to form the uncorrected quadrature component of the LPE signal. In practice, four phase settings 90° apart are used to cancel dc mixer offsets. The 0° and the negative of the 180° measurements are combined to form the in-phase component, and the 90° and the negative of the 270° measurements are combined to form the quadrature component. Note that the LPE signals thus obtained include the frequency response of the receiver and are therefore uncorrected. To obtain corrected LPE signals, the frequency response of the receiver must be removed. The correction procedure required to remove this frequency response is described below.

Among the signals that can be recorded by the measurement approach are the input and output waveforms of a nonlinear device-under-test (DUT). The signal source and the receiver are connected together to record the input LPE signal, and the DUT is inserted between the source and the receiver to record the output LPE signal. Another application of this technique is to record the output waveforms of microwave-frequency modulators. These time-domain measurements can then be used to optimize and validate simulation models of these components and systems.

To enhance the usefulness of the time-domain measurement system, an upconverting transmitter is also included that can be used with an LO source coherent to the receiver LO, and a baseband waveform synthesizer, to provide modulated microwave signals defined by the user. The transmitter is illustrated in Fig. 2. The microwave amplifier and variable attenuator are provided to allow the input power to the DUT to be adjusted over its operating range.

Once the uncorrected signals are obtained, the receiver frequency response must be analytically removed. The receiver frequency response is measured by means of the baseband double-sideband mixer characterization method [3]. The setup for this method consists of an upconverting transmitter followed by a downconverting receiver that both use the same LO and have a phase shifter in the LO path, as shown in Fig. 1. A vector network analyzer (VNA) is used to measure this combination at two relative phase settings 90° apart. The two measurements can be mathematically combined to provide the frequency response of the transmitter and receiver pair. They are not sufficient to extract the frequency response of the receiver alone.

To calculate the response of the receiver, two additional similar configurations using a third frequency converter (a test mixer) are required. The second configuration consists of the test mixer used as an upconverting transmitter followed by the receiver, and the third configuration consists of the transmitter followed by the test mixer used as a downconverter. The method requires that the test mixer have the same frequency response whether it is used as an upconverter or a downconverter. In practice, commonly available double-balanced mixers exhibit this reciprocal response if a low VSWR is provided on all ports by means of fixed attenuators. By mathematically combining the six measurements provided by the three setups, the LPE frequency response of the receiver can be obtained to within a fixed phase offset. This response is then removed analytically from the uncorrected LPE signal measurements, leaving an accurate LPE representation of the microwave signal. Note that the frequency response of the MTA has not been removed from these measurements.

III. Comparison of Baseband Technique with Direct Microwave Measurement

Although any modulated signal may be used to validate our technique, we used a 0.35-ns width, 0.5-V amplitude baseband pulse as the modulation input to the transmitter. The LO frequency was 19.6 GHz. The transmitted pulse was measured using our baseband time-domain measurement technique and the receiver correction was applied. As a validation of our baseband technique, the same signal was measured directly at 19.6 GHz using the MTA. Fig. 3 shows the signal envelope of both the corrected and uncorrected baseband measurement and the directly measured microwave pulse at 19.6 GHz.

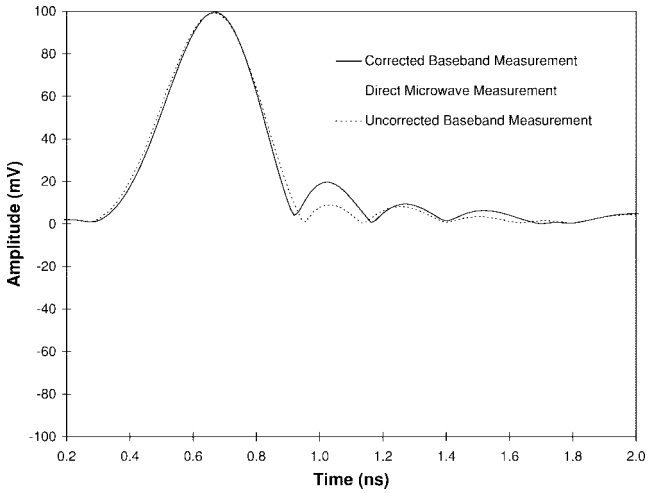

Fig. 3. Comparison of time-domain measurement techniques applied to a microwave pulse.

The excellent agreement between the corrected baseband and the direct microwave measurements indicates the validity of the baseband measurement technique. The disagreement of the uncorrected baseband measurement with the other two measurements indicates the validity of the corrections applied to remove the response of the receiver. Fig. 4 compares the same three measurements after transformation to the frequency domain. The maximum deviation between the corrected baseband and the microwave measurements is $\pm 3°$ and ± 0.4 dB across a 4-GHz bandwidth (except at the dc frequency where the power spectral density is low, so that the error is larger). This comparison illustrates the consistency of the baseband technique with the direct measurement. For this simple case, either the direct microwave or baseband measurements yield acceptable waveform data.

Measuring signals at baseband has several advantages compared to measuring them directly at the carrier frequency. One is that the sample rate can be reduced by the ratio of half the signal bandwidth to the carrier frequency, thereby allowing for a longer time record or higher time resolution of the signal for the same number of samples. This is particularly important when the repetition period of the signal is too long to allow Nyquist sampling of the signal at the carrier frequency, given the limited number of samples available (1024 samples for the MTA). Another advantage is that the time base accuracy and stability requirements for the MTA are reduced by the same ratio of half the signal bandwidth to the carrier frequency. Another improvement is that the phase noise of the carrier is eliminated since the same LO is used for both the upconversion and the downconversion. Also, with an appropriate downconverter, measurements can be done at carrier frequencies beyond the upper frequency limit of the MTA (40 GHz). Finally, the MTA has a flatter frequency response at baseband than at high carrier frequencies (Fig. 5). For example, signals with a 4-GHz bandwidth require only 2 GHz at baseband, over which the MTA has a gain variation of only ± 0.1 dB. The phase deviation from linearity can be as high as 40° for a typical digitizing oscilloscope at 20 GHz, but it is negligible below 5 GHz [4].

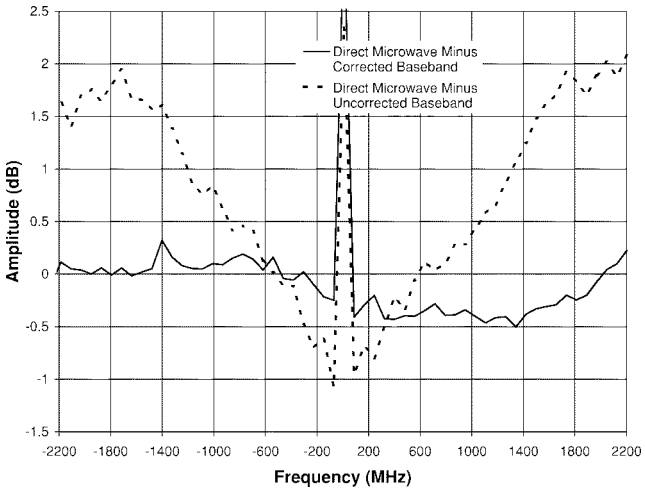

(a)

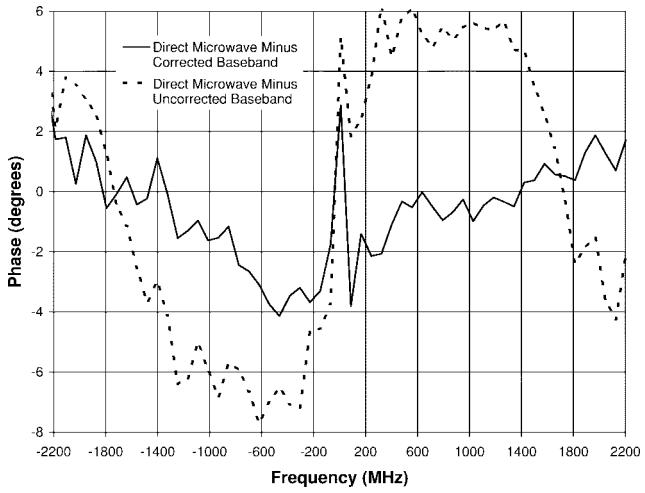

(b)

Fig. 4. Comparison of time-domain measurement techniques applied to a microwave pulse transformed to the frequency domain. The direct microwave measurement has been downconverted to baseband in software. (a) Comparison of measurement amplitudes. (b) Comparison of measurement phases.

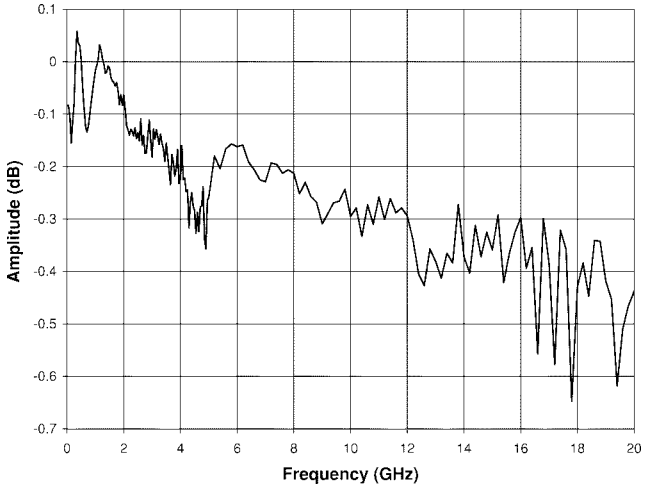

Fig. 5. MTA amplitude response calibration using an HP8485D Power Sensor as a "gold" standard.

IV. Wideband Signal Measurements of a Nonlinear Power Amplifier

The baseband waveform measurement technique described above was applied to measure the input and output waveforms of a 20-GHz TWTA. A number of different wideband waveforms were recorded, including low-duty cycle pulse trains and continuously digitally modulated signals. Low-duty cycle pulses are ideal for discerning the distortion created by nonlinear amplification [5]. These time-domain input/output waveforms clearly identify the compression, pulse broadening, and ringing effects associated with power amplifiers. The initial development of nonlinear models is also facilitated using such pulses since optimization can be performed on a relatively few number of samples. Continuously digitally modulated signal waveforms are longer in time duration and are commonly used in system performance predictions. A wideband digitally modulated signal that has a nonconstant envelope is a good test for nonlinear model fidelity.

The low-duty cycle pulse waveforms were created using on/off keying (OOK) and binary phase-shift keying (BPSK) modulation. The OOK pulse is created by simply applying a unipolar amplitude pulse to the upconverting mixer in the test system transmitter. A bipolar amplitude pulse is used to create the BPSK pulse. The 0.35-ns wide pulse input to the transmitter is broadened to approximately 0.7 ns at the input to the amplifier DUT. The bandwidth of this pulse input was intentionally limited to span the operational bandwidth of the TWTA. Data was taken at a sampling rate of 19.53 ps with an averaging factor of 64. The measured in-phase and quadrature waveforms were converted to polar form (envelope amplitude and phase) for modeling purposes. Note that the dc level of the envelope amplitude indicates the operating point (average level of the RF carrier) on which the pulse is imposed. The operating point of most interest is at or near saturation where the TWTA operates with high power efficiency.

The amplitude and phase envelopes of the OOK pulse are shown in Fig. 6. The amplitude envelope covers a wide dynamic range as it approaches 0 V and returns to the dc steady-state (saturation) condition. The phase envelope of the OOK pulse is almost constant, as it deviates only by $\pm 10^\circ$ maximum. The amplitude and phase envelopes of the BPSK pulse are shown in Fig. 7, where the nonideal switching between the $0^\circ/180^\circ$ phase states is apparent. An ideal BPSK signal would transition to 0 V and back to the dc saturation level in a much shorter time than the duration in the 180° phase state. The phase envelope shows that only approximately 140° of the desired 180° of phase shift is attained during the pulse duration.

A digitally modulated signal can be classified in terms of its amplitude envelope fluctuations. Constant envelope signals such as minimum-shift keying (MSK) are ideal for use with nonlinear amplification. With no amplitude envelope fluctuations present, no AM/AM or AM/PM distortion is imparted on the output signal. In practical applications, however, nonideal circuitry in or after the modulator will create a nonconstant envelope prior to the transmit amplifier. There are also many instances where nonconstant envelope modulation must be used with nonlinear amplification (e.g., a bandwidth efficient scheme such as 16-ary quadrature amplitude modulation). It is therefore essential to characterize amplifier models with the stressing case of nonconstant envelope signals. For this work, a nonideal MSK signal with a nonconstant envelope was used.

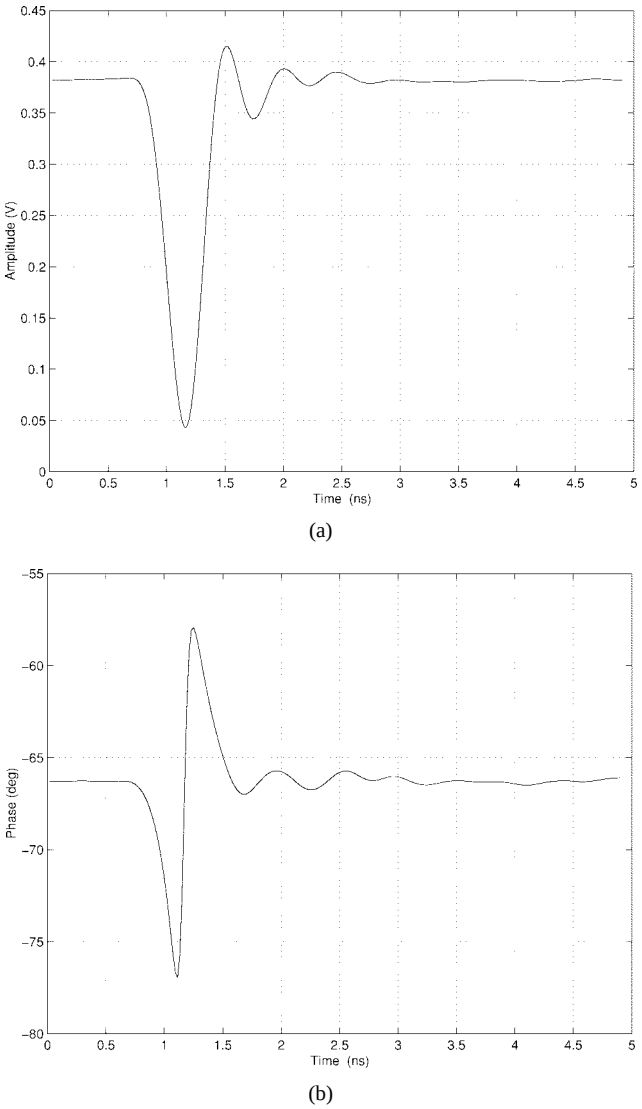

Fig. 6. (a) OOK pulse input amplitude envelope. (b) OOK pulse input phase envelope.

A 5-ns segment of the measured input amplitude and phase envelopes of the MSK waveform is shown in Fig. 8. This is only approximately 8 bits of the 64-bit pseudorandom noise (PRN) sequence that was recorded. Data samples were taken at a rate of 39.06 ps using an averaging factor of 64. The average dc level of the amplitude envelope shown corresponds to the input power at saturation. The amplitude envelope has adequate variations to stress the nonlinearity. The high data rate (0.35-ns bit duration) provides for the rapidly time-varying envelope. The phase envelope is also continuously varying as it goes through a full 360° rotation four times during the 8-bit sequence shown.

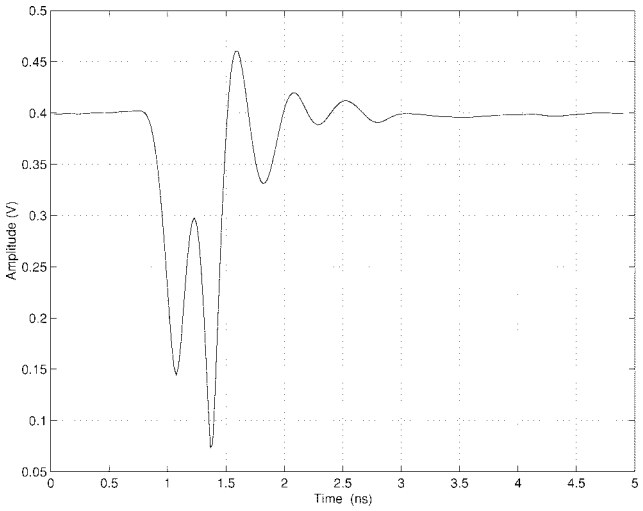

(a)

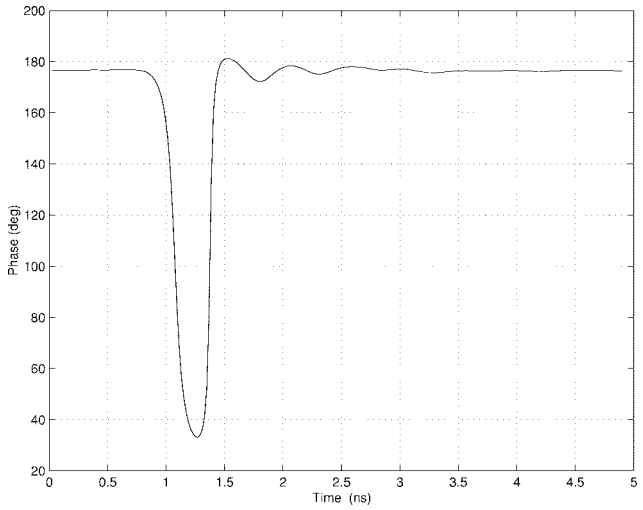

(b)

Fig. 7. (a) BPSK pulse input amplitude envelope. (b) BPSK pulse input phase envelope.

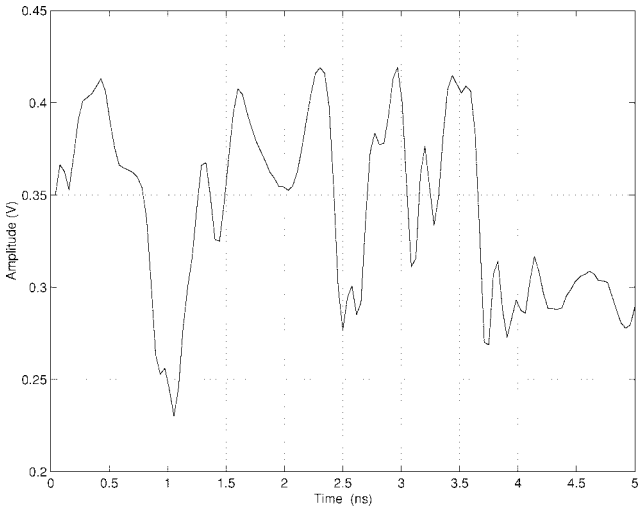

(a)

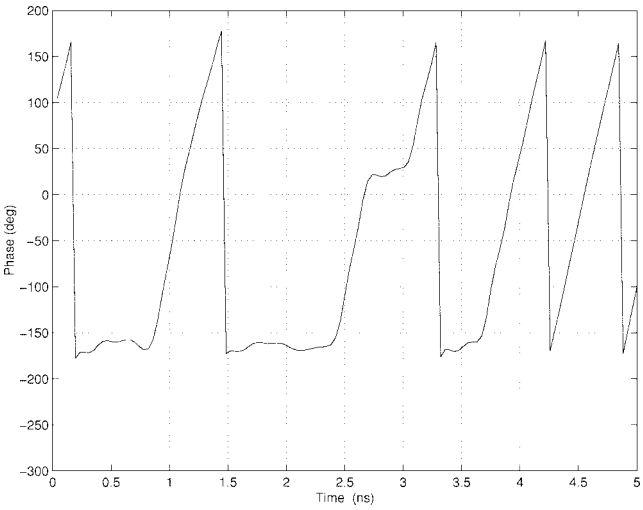

(b)

Fig. 8. (a) MSK input amplitude envelope. (b) MSK input phase envelope.

V. Model Development

The wideband signals described above are employed to optimize a wideband TWTA model. The commonly used memoryless envelope model, in which the nonlinear device is completely described by the AM/AM and AM/PM transfer functions, was also generated for comparison. The AM/AM and AM/PM transfer functions are obtained using a VNA and a single-tone power sweep at the center operating frequency [6]. The complex output h of the memoryless envelope model is given by

$$h = h(A) = g(A)e^{j[\phi(A)+\theta]} \tag{1}$$

where $A = A(t)$ is the amplitude of the complex input envelope, $\theta = \theta(t)$ is its arbitrary phase, and $g(\cdot)$ and $\phi(\cdot)$ are the AM/AM and AM/PM transfer functions, respectively. To enable the optimization of the nonlinearity presented in (1), we re-expressed the two associated transfer functions in analytical form through a finite Bessel-series expansion consisting of only odd-order terms, as follows:

$$g(A) = \sum_{i=1}^{L} c_{2i-1} J_1[(2i-1)\alpha A] \tag{2a}$$

$$\phi(A) = \sum_{i=1}^{L} d_{2i-1} J_1[(2i-1)\alpha A] \tag{2b}$$

where α is a normalizing constant, and $J_1[\cdot]$ is the first-order Bessel function of the first kind. The real coefficients $\{c_i\}$ and $\{d_i\}$ are determined by an optimization technique based on the method of least squares. The measured data and corresponding seven-term Bessel series representation of the TWTA characteristics are shown in Fig. 9. The nonlinearity can also be represented in an equivalent quadrature form.

The new nonlinear amplifier model developed in this paper is an extension of the memoryless envelope model that includes an auto-regressive moving average (ARMA) filter at the input. As shown in Fig. 10, the Nth-order ARMA model

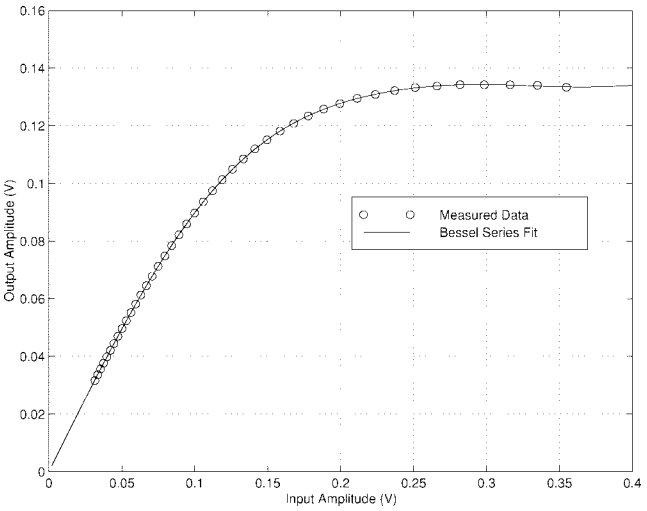

(a)

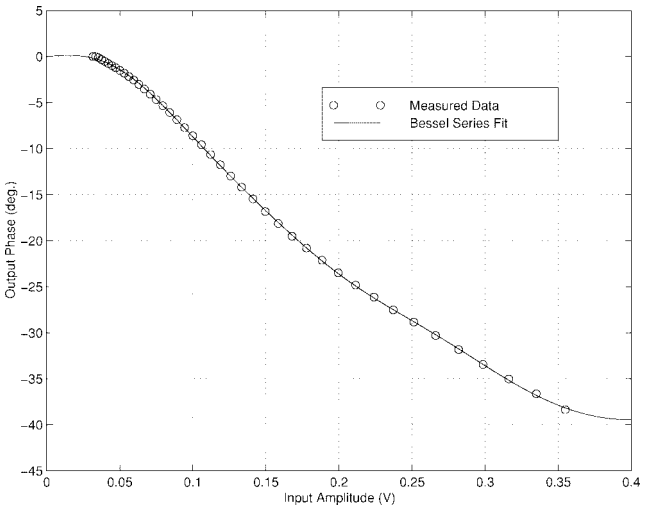

(b)

Fig. 9. (a) TWTA AM-AM characteristic. (b) TWTA AM-PM characteristic.

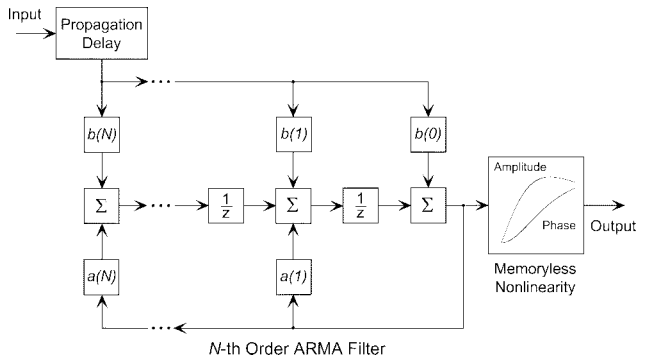

Fig. 10. Nonlinear ARMA model.

is an infinite impulse-response (IIR) structure consisting of N unit delay sections. The filter operates on the complex, LPE envelope, each section consisting of a feed-forward and a feedback path with complex coefficients. The incorporation of feedback allows for versatile modeling capability in a compact structure.

The input-output relation of the ARMA filter can be expressed recursively as

$$y(k) = \sum_{i=0}^{N} b_i x(k-i) - \sum_{i=1}^{N} a_i y(k-i) \tag{3}$$

where $x(m)$ and $y(m)$ denote the complex mth sampled input and output of the filter at time mT_s, respectively, and $1/T_s$ is the sampling rate. The coefficients $\{a_i\}$ and $\{b_i\}$ are complex scalars that define the model. The memoryless nonlinearity defined in (1) and (2) is placed after the ARMA filter to complete the model. The model approximates the physical operation of the TWTA since the compression occurs near the output as the signal travels down the traveling-wave structure.

Although the model could be generated using only time-domain measurements, VNA-based frequency-domain measurements were also used. In order to derive the model coefficients for the nonlinear model, a numerical optimization procedure is required. The numerical algorithm is very sensitive to the initial conditions which determine whether the solution converges to a global or local minimum. Therefore, the initial values of the ARMA model are derived for the linear case before the numerical optimization algorithm is performed. The initial values of the filter coefficients were chosen to represent the small-signal (linear) response of the TWTA. Applying a fast Fourier transform (FFT) analysis to the VNA measured transfer function, the time-domain output $[y_o^l(k)]$ was calculated. A closed-form solution for the coefficients was obtained by minimizing the mean-squared error (MSE) between measured and modeled time-domain outputs. Using (3) with measured small-signal input data $[x_{\text{meas}}^l(k)]$ placed in its right-hand side, the error function $\epsilon(k)$ between the measured small-signal $[y_{\text{meas}}^l(k)]$ and the modeled $[y_{\text{mod}}^l(k)]$ output response can be defined as

$$\epsilon(k) := y_{\text{mod}}^l(k) - y_{\text{meas}}^l(k) \tag{4a}$$

$$= \sum_{i=0}^{N} b_i x_{\text{meas}}^l(k-i) - \sum_{i=1}^{N} a_i y_o^l(k-i) - y_{\text{meas}}^l(k). \tag{4b}$$

Because the derivation of the filter coefficients is facilitated by using matrix notation, we rewrite the error function in the following vector format:

$$\epsilon(k) = \boldsymbol{w}^H \boldsymbol{z}_k - y_{\text{meas}}^l(k) \tag{5a}$$

where the complex coefficient vector $\boldsymbol{w}$ and data vector $\boldsymbol{z}_k$ in (5a) are defined as

$$\boldsymbol{w} := [b_0, \cdots, b_N, -a_1, \cdots, -a_N]^H \tag{5b}$$

and

$$\boldsymbol{z}_k := [x_{\text{meas}}^l(k), \cdots, x_{\text{meas}}^l(k-N), y_o^l(k-1), \cdots, y_o^l(k-N)]^T \tag{5c}$$

where $(\cdot)^H$ denotes conjugate transposition and $(\cdot)^T$ denotes ordinary transposition. The minimum MSE is obtained by taking the gradient of the objective function with respect to

the coefficient vector and setting the result equal to zero, that is,

$$\nabla_{\boldsymbol{w}}\left[\sum_{k=1}^{M}|\epsilon(k)|^2\right]=0 \tag{6}$$

where the sum is taken over M data samples. Defining the data matrix $\boldsymbol{Z}$ and vector $\boldsymbol{\chi}$ as

$$\boldsymbol{Z}:=\sum_{k=1}^{M}\boldsymbol{z}_k\boldsymbol{z}_k^H \tag{7a}$$

$$\boldsymbol{\chi}:=\sum_{k=1}^{M}\left[y_o^l(k)\right]^*\boldsymbol{z}_k \tag{7b}$$

the solution to (6) can be shown to be given by

$$\boldsymbol{w}=\boldsymbol{Z}^{-1}\boldsymbol{\chi}. \tag{8}$$

This solution allows for the determination of the model order for linear operation and provides a lower bound on the filter order for nonlinear operation. An eleventh-order ARMA model was sufficient for the subsequent nonlinear optimization on OOK and BPSK pulse waveforms. A 23rd-order model was required for similar accuracy for the continuously MSK-modulated waveforms. The initial condition for the AM/AM and AM/PM characteristics were identical to those used in the memoryless envelope model.

Combining (1)–(3), and denoting the output of the ARMA filter by $y_{\mathrm{mod}}^n(k)$ when the input is the large-signal $x_{\mathrm{meas}}^n(k)$, the input-output relation for the ARMA filter-nonlinearity concatenation can be expressed as (9a)–(9c), shown at the bottom of this page, where the superscript n indicates a nonlinear regime of operation,

$$\begin{aligned}\tilde{\boldsymbol{w}}:=&[b_{0I},\cdots,b_{NI},b_{0Q},\cdots,b_{NQ},a_{1I},\cdots,a_{NI},\\&a_{1Q},\cdots,a_{NQ},c_1,\cdots,c_{2L-1},d_1,\cdots,d_{2L-1}]^T\end{aligned} \tag{10}$$

represents the $2(2N+L+1)$ coefficients of the complete model

$$\begin{aligned}\tilde{\boldsymbol{z}}_k:=&\left[x_I^n(k),\cdots,x_I^n(k-N),x_Q^n(k),\cdots,x_Q^n(k-N),\right.\\&y_{\mathrm{mod,\,I}}^n(k-1),\cdots,y_{\mathrm{mod,\,I}}^n(k-N),\\&\left.y_{\mathrm{mod,\,Q}}^n(k-1),\cdots,y_{\mathrm{mod,\,Q}}^n(k-N)\right]^T\end{aligned} \tag{11}$$

represents the past inputs and outputs, as well as the current input [$2(2N+1)$ samples total], and we have decomposed all complex scalars into a real or in-phase part (subscripted with I) and an imaginary or quadrature part (subscripted with Q). The model coefficients of both the ARMA filter and nonlinearity were optimized numerically—using a steepest descent (Levenberg-Marquardt) least-squares algorithm [7]—to minimize the MSE between the modeled and measured waveform data. The objective function for the nonlinear numerical optimization can be expressed as

$$\begin{aligned}\min_{\tilde{\boldsymbol{w}}}\{\mathrm{MSE}\}=\min_{\tilde{\boldsymbol{w}}}\left\{\sum_{k=1}^{M}\left([r_{\mathrm{mod,\,I}}(k;\tilde{\boldsymbol{w}},\tilde{\boldsymbol{z}}_k)-r_{\mathrm{meas},\,I}(k)]^2\right.\right.\\\left.\left.+[r_{\mathrm{mod,\,Q}}(k;\tilde{\boldsymbol{w}},\tilde{\boldsymbol{z}}_k)-r_{\mathrm{meas},\,Q}(k)]^2\right)\right\}.\end{aligned} \tag{12}$$

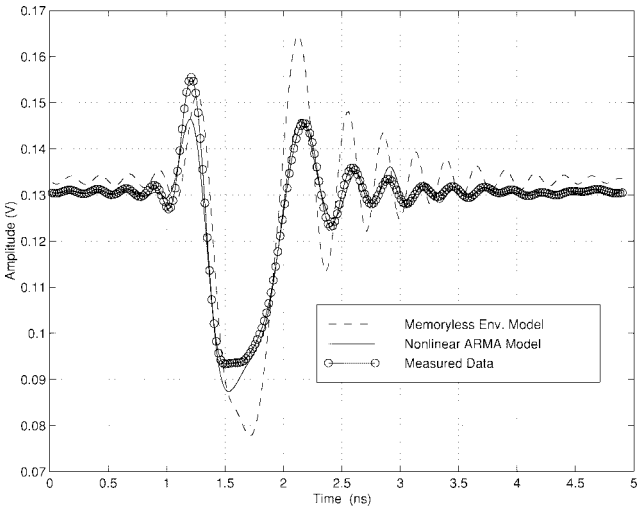

(a)

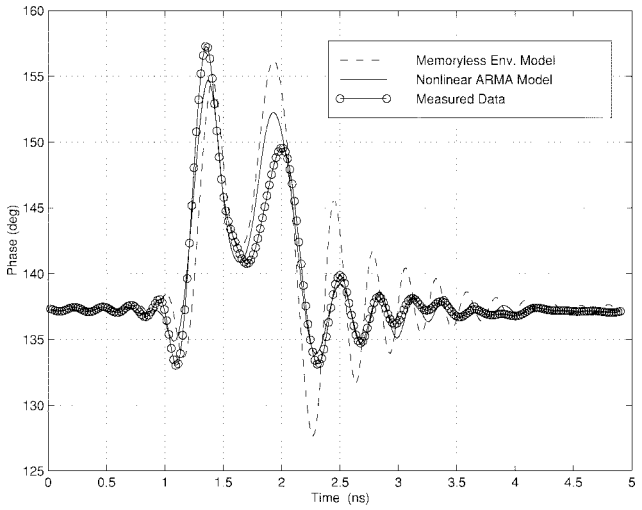

(b)

Fig. 11. (a) Model comparison of OOK pulse output amplitude envelopes. (b) Model comparison of OOK pulse output phase envelopes.

$$r_{\mathrm{mod}}(k):=h(|y_{\mathrm{mod}}^n(k)|) \tag{9a}$$

$$=\sum_{i=1}^{L}c_{2i-1}J_1[(2i-1)\alpha|y_{\mathrm{mod}}^n(k)|]\times\exp\left\{j\left(\sum_{i=1}^{L}d_{2i-1}J_1[(2i-1)\alpha|y_{\mathrm{mod}}^n(k)|]+\theta\right)\right\} \tag{9b}$$

$$=:r_{\mathrm{mod,\,I}}(k;\tilde{\boldsymbol{w}},\tilde{\boldsymbol{z}}_k)+j\,r_{\mathrm{mod,\,Q}}(k;\tilde{\boldsymbol{w}},\tilde{\boldsymbol{z}}_k) \tag{9c}$$

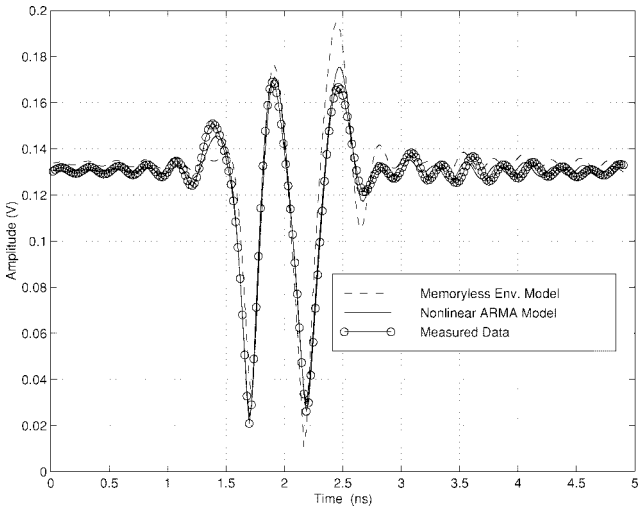

(a)

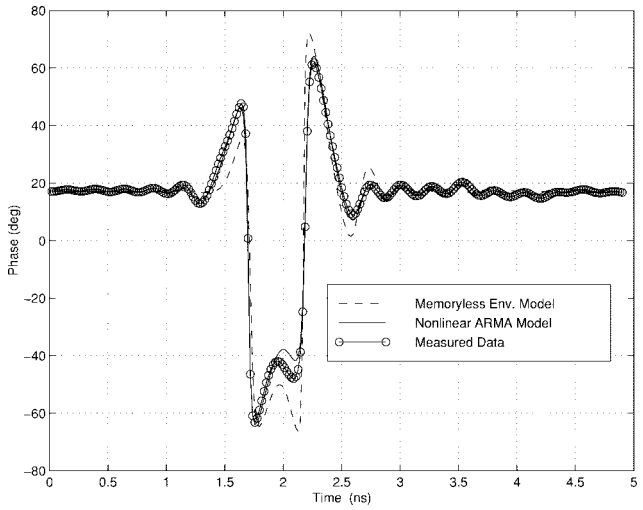

(b)

Fig. 12. (a) Model comparison of BPSK pulse output amplitude envelopes. (b) Model comparison of BPSK pulse output phase envelopes.

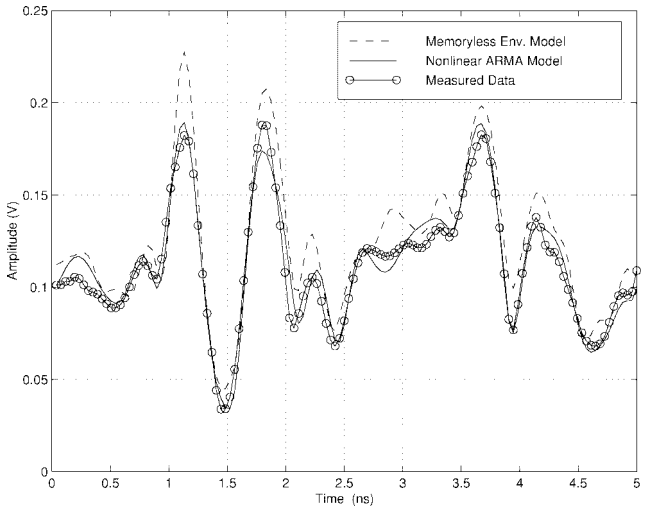

(a)

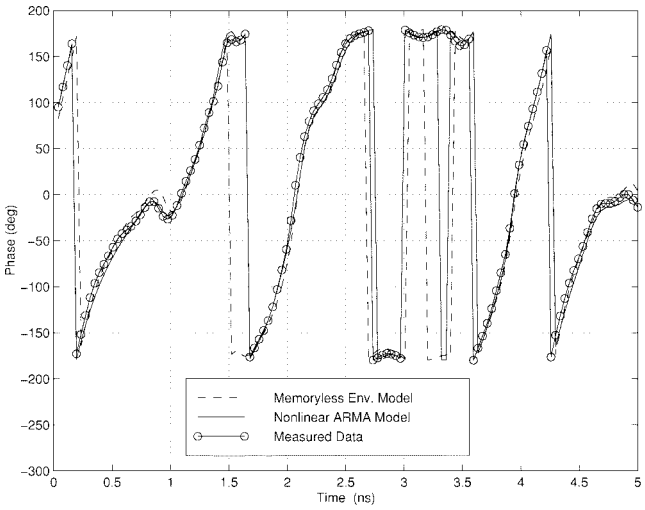

(b)

Fig. 13. (a) Model comparison of MSK output amplitude envelopes. (b) Model comparison of MSK output phase envelopes.

The optimization metric was chosen to produce a model that would provide an improvement in end-to-end systems symbol error-rate calculations for digitally modulated signals. The error-vector-magnitude (EVM), which is the square root of the summand in (12), is therefore minimized at each time sample over the full length of the waveform. The normalized MSE (NMSE) is calculated by dividing by the total signal power in the measured waveform:

$$\text{NMSE} := \frac{\text{MSE}}{\sum_{k=1}^{M}\left[r^2_{\text{meas},I}(k) + r^2_{\text{meas},Q}(k)\right]}. \qquad (13)$$

The NMSE can be used as a figure of merit for model accuracy over a range of possible operating conditions. Since waveform EVM directly corresponds to possible symbol errors, the NMSE can, in some cases, be used to estimate the model's ability to predict symbol error-rate. This is discussed in more detail in relation to model accuracy with MSK waveforms.

VI. Model Comparison

Results from the nonlinear ARMA model are first compared to those from the memoryless envelope model for low-duty cycle pulses. Fig. 11 compares the model outputs to measured data for the OOK pulse. The eleventh-order nonlinear ARMA model follows the measured data more closely than the memoryless envelope model. The NMSE is 0.91% and 7.66% for the nonlinear ARMA and memoryless envelope models, respectively. Fig. 12 compares the model output results to measured data for the BPSK pulse. Note the difference in scale between the OOK and BPSK pulse outputs. Fig. 12(b) clearly shows the effect of nonlinear distortion as the peak phase shift from saturation is decreased from 140° to approximately 80°. For the BPSK pulse, the NMSE is 1.85% and 13.18% for the nonlinear ARMA and memoryless envelope models, respectively. Note that for these signals, the MSE normalization is based on single pulse power.

Results from both models are also compared for the MSK signal. Fig. 13 compares the memoryless and twenty-third-

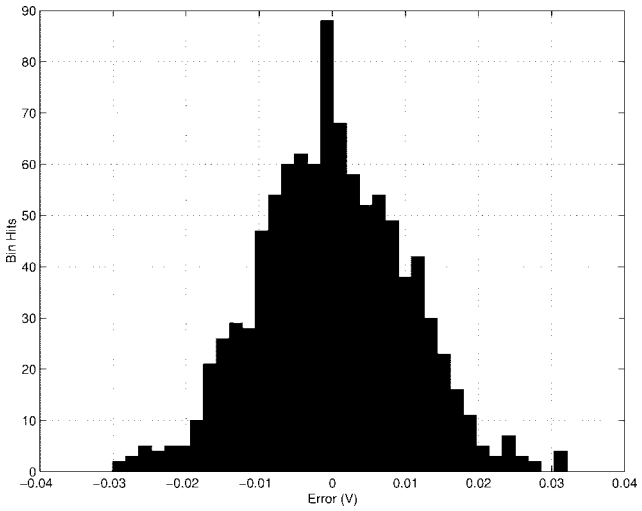

Fig. 14. Histogram of MSK in-phase waveform errors (35 bins).

order nonlinear ARMA model outputs to the measured data. The 64-bit NMSE is 1.11% and 4.26% for the nonlinear ARMA and memoryless envelope models, respectively. In this case the MSE normalization is based on the total power in the 64-bit sequence. The MSK waveform NMSE calculations provide a better indication of symbol error-rate than the single pulse calculations since they are based on a full 64-bit PRN pattern. A simple uncertainty estimate for the symbol error rate due to a specified NMSE can be made if the waveforms errors are Gaussian distributed. The histogram of the MSK in-phase waveform errors shown in Fig. 14 closely resembles a Gaussian distribution. These waveform errors can be considered as an equivalent noise power that can either add or subtract from the actual system noise to produce an equivalent system noise power for calculation of symbol error probability. For BPSK, for example, a 4% NMSE would cause a 2.2-dB uncertainty at a 10-dB actual signal-to-noise ratio, whereas a 1% EVM NMSE would only cause a 0.5-dB uncertainty.

VII. Conclusion

A new method to measure microwave signals in the time domain by first downconverting to baseband has been presented. This new technique does not suffer the accuracy and noise limitations of measurements performed directly at the carrier frequency. Accurate low-pass equivalent waveforms are obtained after correcting for the receiver response by means of the baseband double-sideband frequency-translating device measurement technique. This technique was applied in the measurement of input/output waveforms for a 20-GHz TWTA subject to a wideband signal input. From these measurements, a new nonlinear model with memory was developed for a TWTA. This new model was found to be more accurate in predicting the response to wideband low-duty cycle pulses and continuously digitally modulated signals.

Acknowledgment

The authors would like to thank Dr. J. D. Michaelson, Dr. K. M. Soo Hoo, and Dr. J. H. Spriggs for their generous support and guidance during the development of this work.

References

[1] M. C. Jeruchim, P. Balaban, and K. S. Shanmugan, *Simulation of Communication Systems.* New York: Plenum, 1992.
[2] M. Schwartz, W. R. Bennet, and S. Stein, *Communication Systems and Techniques.* New York: IEEE Press, pp. 35–43, 1966.
[3] C. J. Clark, A. A. Moulthrop, M. S. Muha, and C. P. Silva, "Transmission response measurements of frequency translating devices using a vector network analyzer," *IEEE Trans. Microwave Theory Tech.*, vol. 44, pp. 2724–2737, Dec. 1996.
[4] J. Verspecht and K. Rush, "Individual characterization of broadband sampling oscilloscopes with a nose-to-nose calibration procedure," *IEEE Trans. Instrum. Measure.*, vol. 43, pp. 347–354, Apr. 1994.
[5] M. I. Sobhy, E. A. Hosny, M. W. R. Ng, and E. A. Bakkar, "Nonlinear system and subsystem modeling in time domain," *IEEE Trans. Microwave Theory Tech.*, vol. 44, pp. 2571–2579, Dec. 1996.
[6] O. Shimbo, *Transmission Analysis in Communication Systems.* Rockville, MD: Computer Science Press, 1988, vol. 2.
[7] W. H. Press, S. A. Teukolsky, W. T. Vetterling, and B. P. Flannery, *Numerical Recipes in C: The Art of Scientific Computing*, 2nd ed. New York: Cambridge University Press, 1992.

Christopher J. Clark was born in Washington, DC, in 1960. He received the B.S. and M.S. in degrees in electrical engineering from the University of Maryland, College Park, in 1983 and 1986, respectively.

From 1984 to 1986 he worked for the Watkins–Johnson Company, where he was responsible for the design and development of RF receiving systems. From 1986 to 1992, he worked for TRW Inc., where he developed microwave components for satellite applications. His primary focus was in the design of MESFET, HEMT, and HBT GaAs MMIC's for phased-array systems. He is currently an Engineering Specialist in the Electromagnetic Techniques Department, Communications Systems Subdivision, at The Aerospace Corporation, Los Angeles, CA. His work involves the design of space communications systems and the development of hardware for digital satellite communications.

Mr. Clark is a member of Eta Kappa Nu and Tau Beta Pi.

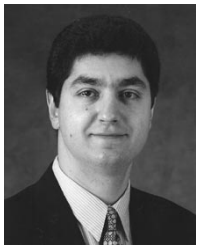

George Chrisikos (M'92) was born in Salonika, Greece, in 1967. He received the B.S. degree in electrical engineering from the University of New Mexico, Albuquerque, in 1989 and the M.S. degree in electrical engineering from the University of Southern California, Los Angeles, in 1991. He is also pursuing the Ph.D. degree in electrical engineering at the latter institution.

He is currently a Senior Member of the Technical Staff in the Electromagnetic Techniques Department, Communications Systems Subdivision, at The Aerospace Corporation, Los Angeles, CA. His work involves digital communications systems design for satellite applications.

Mr. Chrisikos is a member of Tau Beta Pi, Eta Kappa Nu, Phi Kappa Phi, and Kappa Mu Epsilon.

Michael S. Muha was born in Inglewood, CA, on February 21, 1958. He received the B.S. degree in physics in 1979 from the University of Southern California, Los Angeles, and the M.S. degree in applied physics in 1981 from the California Institute of Technology, Pasadena, where he worked on the design and development of millimeter-wave and far-infrared imaging antenna arrays.

He is currently Manager of the Communication Techniques Section in the Electromagnetic Techniques Department at The Aerospace Corporation, Los Angeles, CA, where he is working on the design, development, and characterization of high-data-rate microwave communications systems.

Mr. Muha is a member of Phi Beta Kappa and Phi Kappa Phi.

Andrew A. Moulthrop was born in San Francisco, CA, in 1955. He received the B.A. degree in physics in 1977 from the University of California, San Diego, and the Ph.D. degree in physics in 1984 from the University of California, Berkeley.

He is currently an Engineering Specialist in the Microwave/Millimeter-Wave Electronics Section in the Electromagnetic Techniques Department at The Aerospace Corporation, Los Angeles, CA. His work involves the design, development, and measurement of microwave components and systems. Previously, he worked as a Research Assistant at the University of California, Berkeley, where he codeveloped a Josephson junction parametric amplifier, as well as measured various properties of superfluid helium.

Dr. Moulthrop is a member of Phi Beta Kappa.

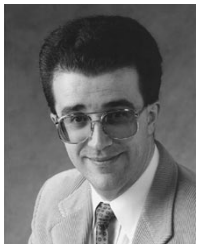

Christopher P. Silva (S'81–M'89–SM'98) was born on March 17, 1960, in Fortuna, CA. He received the B.S., M.S., and Ph.D. degrees, all in electrical engineering, in 1982, 1985, and 1993, respectively, from the University of California, Berkeley. His graduate work was supported mainly by a National Science Foundation Fellowship and a Lockheed Leadership Fellowship.

He is currently a Senior Member of the Technical Staff of the Electromagnetic Techniques Department, Communications Systems Subdivision, at The Aerospace Corporation, Los Angeles, CA. He has been the principal investigator on several internally funded research projects addressing nonlinear microwave CAD, secure communications by means of chaos, and compensation of nonlinear satellite communications channels. In addition, he is currently heading a study on the nonlinear modeling and compensation of high-data-rate microwave communications systems in support of national advanced satellite programs. He is also involved with the application of wavelet analysis to CAD and communications signaling. Previously, he worked as a Post Graduate Researcher at the Electronics Research Laboratory, University of California, Berkeley, where he investigated the chaotic dynamics of nonlinear circuits and systems.

Dr. Silva is a member of Eta Kappa Nu, Tau Beta Pi, Phi Beta Kappa, the Society for Industrial and Applied Mathematics, the American Mathematical Society, the American Institute of Aeronautics and Astronautics, and the American Association for the Advancement of Science.